Available online at www.sciencedirect.com
ScienceDirect
Trans. Nonferrous Met. Soc. China 34(2024) 533−546
Transactions of Nonferrous Metals Society of China
www.tnmsc.cn

Vibration fatigue properties and deterioration mechanism of diffusion bonded TC4 titanium alloy

Yi-wen LEI[1], Guang-lu MA[2], Yue LIU[2], Wei ZHAO[2], Hui-ping WU[1], Xi-feng LI[1]

1. Institute of Forming Technology & Equipment, School of Materials Science and Engineering, Shanghai Jiao Tong University, Shanghai 200030, China;
2. AECC Shenyang Liming Aero Engine (Group) Co., Ltd., Shenyang 110043, China

Received 27 June 2022; accepted 14 October 2022

Abstract: To analyze the effect of diffusion bonding process on vibration fatigue properties, a series of fatigue tests and microstructure characterization of as-received and diffusion bonded TC4 titanium alloy were conducted. The results show that the thermal cycling of diffusion bonding process results in microscopic change and deteriorates vibration fatigue lifetime of TC4 alloy. For bonded TC4 alloy, the increased grain size inhomogeneity stimulates incompatible deformation of differently oriented α grains and leads to micro-void formation at boundaries of small/large α grain pairs or inside large α grains. Meanwhile, the orientation variation of α grains promotes activation of prismatic slip systems for earlier crack initiation. In addition, the increased fraction of β phase provides more nucleation locations for micro-voids. Thus, the increase of the grain size inhomogeneity, grain orientation change, and the increase of β phase fraction due to the thermal cycling result in fatigue performance deterioration of diffusion bonded TC4 titanium alloy.
Key words: diffusion bonding; vibration fatigue; thermal cycling; TC4 titanium alloy

1 Introduction

TC4 titanium alloy owns an excellent combination of strength, toughness, and weldability, which has been widely used in the aerospace field [1−3]. To improve the service properties of titanium alloys, scholars have conducted a lot of research work, such as obtaining work hardened or amorphization layer on Ti−6Al−4V (TC4) surface by peening process [4,5]. However, many TC4 titanium alloy components still suffer from vibration fatigue problems due to the complex cyclic dynamic loading conditions [6]. Vibration has been reported to have a greater impact on fatigue life of compressor blades than cyclic centrifugal force [7]. Since vibration fatigue often results in sudden fracture without large plastic deformation, its characteristics and mechanisms are focused among in-service performance evaluation aspects of titanium alloy.

Diffusion bonding (DB) is a solid-state welding process and an advisable method for manufacturing complex components. Different atoms between the intimately contacted surfaces are sufficiently diffused under high temperature and suitable pressure [8]. Much attention has been paid to the damage tolerance properties of DB interface subjected to low-frequency (<50 Hz) cyclic loading in tension−tension form [9−12]. HE et al [10] found that DB laminates of TC4 alloy with unbonded zone had good damage tolerance properties, since the unbonded zone had significant effect on the deceleration of fatigue crack propagation rate. LI et al [12] investigated the fatigue crack propagation characteristics of TA15/TC4 diffusion-bonded dissimilar laminates and noted that TA15 alloy exhibited a lower fatigue crack growth rate due to

Corresponding author: Xi-feng LI, Tel: +86-21-62830509, Fax: +86-21-62826575, E-mail: lixifeng@sjtu.edu.cn
DOI: 10.1016/S1003-6326(23)66415-5

relatively random α grains orientation compared to TC4 alloy. Most of the current research is focused on the effect of bonded-interface regions on fatigue crack growth rates. Meanwhile, a series of tests [13−15] have shown that diffusion bonded joints with almost no voids on the interface can be obtained under appropriate DB parameters. Therefore, the influence of process factors other than the bonded interface on fatigue properties during diffusion bonding is also worth considering. For example, DB involves a distinct thermal cycling process including heating, holding at DB temperature and furnace cooling to room temperature, during which grain growth [16] as well as microstructure transformation [11] may occur.

It has been confirmed that microstructure characteristics significantly affect the fatigue properties of titanium alloys [17−20]. CAPPOLA et al [17] investigated the behavior of microtextured regions in Ti−6Al−4V (TC4) alloy via crystal plasticity finite element simulations and proved that the presence of microtextured regions caused early fatigue crack nucleation. LUCAS and KONIECZNY [19] noticed that Ti−6Al−4V alloy with finer α grains exhibited higher fatigue strength. In addition, PAN et al [5] found that dislocation multiplication and deformation twinning caused severe grain refinement during warm laser shock peening on Ti−6Al−4V alloy, and fine grains were more stable during fatigue cyclic loading. ZUO et al [20] found that Ti−6Al−4V alloy with basketweave microstructure had lower fatigue strength and larger scatter of fatigue data than that with bimodal one. Fundamental reason for fatigue initiation is the microplasticity caused by irreversible cyclic slip due to microstructure inhomogeneity [21,22]. For TC4 titanium alloy, the stiffness difference between α and β phases leads to incompatible deformation at the microscale, which results in stress concentration at phase boundaries and activation of slip systems in α phase. Soft α phase is reported to be more highly strained than β phase, which causes high local strain concentration [23,24]. Meanwhile, the higher slip length in α grains results in several times faster small-crack growth rates compared with transformed β regions [25]. However, the research on the effect of thermal cycling processes during diffusion bonding on microstructure and fatigue properties is currently lacking.

Current study on fatigue crack initiation mechanism is mainly conducted by in-situ fatigue test combined with characterization methods like DIC (digital image correlation), which may reveal how the first micro-crack initiates [26,27]. However, it is limited to the application in low-frequency uniaxial loading fatigue tests [28−30]. For those fatigue tests that are not easily observed in situ [31,32], the most common method is using the focused ion beam (FIB) technique combined with microstructure characterization to obtain crystallographic information from the specific fracture surfaces and clarify crack initiation mechanism indirectly. Although it enables the explanation of crack initiation mechanism, the FIB technique is complicated and costly to operate. Therefore, it makes sense to find a simpler way to analyze the mechanism for crack initiation, such as taking micro-voids near the main fatigue crack as incompatible deformation indicators for crack initiation.

In this study, the fatigue characteristics of diffusion-bonded TC4 alloy under high-frequency vibration loading were investigated and compared with those of the as-received alloy. The effects of thermal cycling process on microstructure and vibration fatigue properties were discussed in detail.

2 Experimental

The material used in the experiment was hot-rolled and annealed TC4 titanium alloy supplied by Baoti Group Co., Ltd., China, and the chemical composition is listed in Table 1. The as-received alloy was cut into 60 mm × 25 mm × 1 mm sheets. The surfaces to be diffusion bonded were ground progressively by SiC sandpapers from 800 to 2000 grit, and cleaned by the ultrasonic cleaner in acetone. Figure 1 shows a schematic illustration of DB process, which was carried out in the vacuum hot-pressing furnace (~5×10^{-3} Pa) at 900 °C for 30 min under 10 MPa, followed by furnace cooling to room temperature. To obtain the mechanical properties of diffusion bonded joint, tensile and shear tests were performed. The gauge length, width and thickness of tensile samples were 30, 10 and 2 mm, respectively. It should be noted that the loading is parallel to the rolling direction. As for the shear sample, the shearing surface size was 3 mm × 4 mm. Both the tensile and shear tests were

conducted with a constant strain rate of $1\times10^{-3}\ s^{-1}$ three times at room temperature.

Table 1 Chemical composition of TC4 titanium alloy (wt.%)

Al	V	Fe	Ti
5.98	4.25	0.23	Bal.

The vibration fatigue tests were performed by the electro-vibration system at room temperature. The testing specimen geometry is shown in Fig. 2(a). After being ground with SiC sandpaper to 2000# grit, the specimen was cantilever-mounted to the clamp attached to the shaker in Fig. 2(b). The shaker provided a vertical base excitation in thickness direction of the specimen to achieve a resonance state. Before the fatigue test, the first-order natural frequency of the specimen was detected by swept sine. The displacement amplitude of specimen tip was monitored by a laser sensor, and the strain gauge was pasted on the center section of specimen surface to establish the relationship among the displacement amplitude, strain and stress. It should be noted that since a large range of stress fluctuations exist at the maximum stress site, the site with larger stress but relatively flat stress gradient was selected to paste the strain gauge to ensure the strain measurement accuracy.

During the fatigue test, the control system of the shaker ensured that the specimen was always at a first-order bending resonance state with a stress ratio R ($\sigma_{min}/\sigma_{max}$) of −1. To improve the test efficiency, a step-by-step loading method was adopted. That is, if the specimen subjected to the constant stress-based load after a certain number of cycles did not reach the damage criteria, the stress level was raised for subsequent vibration until the fatigue damage occurred. The fatigue damage criterion was a 1% reduction of the initial natural frequency of the specimen corresponding to the cyclic loading varied from 350 to 500 MPa below the macroscopic yield strength. Four specimens were tested, two of which were diffusion-bonded specimens and the other two were as-received specimens for comparison.

The microstructures of diffusion-bonded sample, as-received alloy, and fatigue fracture characteristics were observed. Samples prepared for

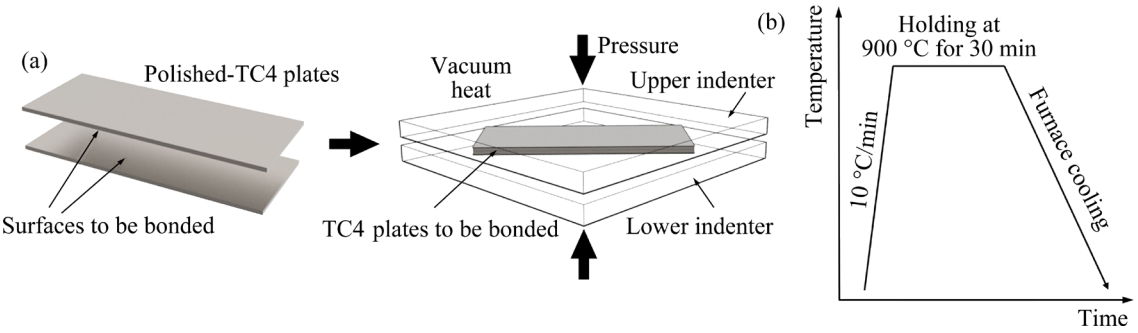

Fig. 1 Schematic diagrams of diffusion bonding process: (a) After surface treatment, TC4 plates heated and pressurized in furnace to get bonded; (b) Thermal cycling during DB process

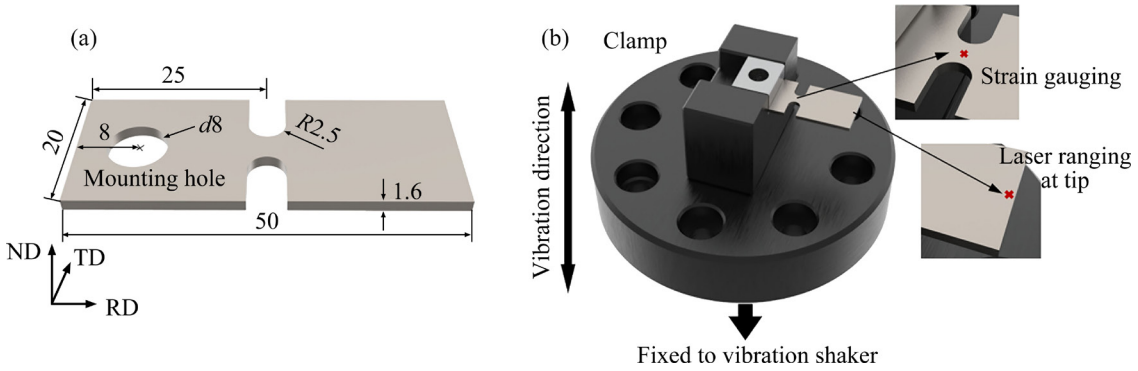

Fig. 2 Specimen geometry (a), and equipment for vibration test (b) (Stress was measured by the strain gauge attached to the surface and the tip amplitude was measured by laser. RD, TD and ND denote the rolling, transverse and normal directions, respectively) (Unit: mm)

optical microscopic (OM) observations were mechanically ground, polished and then etched using 2 mL HF + 4 mL HNO_3 + 94 mL H_2O solution for 10 s. Samples prepared for electron backscatter diffraction (EBSD) and backscattered electron (BSE) observations needed extra vibration polishing for 3 h to remove the surface residual stress layer caused by mechanical grinding. The fatigue fracture surfaces were cleaned using acetone and then observed by scanning electron microscopy (SEM). SEM observations were performed with an accelerating voltage of 5 kV. EBSD tests were carried out with an accelerating voltage of 20 kV and a step size of 0.1 μm. BSE experiments were conducted at 20 kV and 7 mm working distance.

3 Results

3.1 Microstructures and mechanical properties

Figure 3 presents the microstructure of the as-received and bonded TC4 titanium alloys. Both of them are composed of equiaxed α phase (white in OM image) and β phase (dark in OM image) along α phase boundaries. As shown in Figs. 3(b) and (d), no obvious void is observed at the bonded interface, which indicates excellent DB quality. Different α grains are distinguished by grain boundaries (shown as black lines) and grain orientations (shown as different colors) in Figs. 3(c, d). It can be seen that α grains grew significantly after DB process, together with the appearance of coarse bar-shaped α grains. Grain size distributions calculated by Channel5 software are shown in Figs. 4(a, b). After DB process, the average size of α grains increases by 29% from 5.2 to 6.7 μm, and the average size of β grains increases by 64% from 1.1 to 1.8 μm. The standard deviation in Table 2 shows that the non-uniformity of grain size is greatly raised. The volume fraction of β phase accounts for 11.7% in as-received alloy and 16.2% in DB sample based on ImageJ software measurement. Thus, a partial $\alpha \rightarrow \beta$ phase transformation occurred during DB process.

As shown in Fig. 3(d), there are some fine recrystallized grains (marked by white squares) at the grain boundaries and inside larger α grains. Meanwhile, it can be found in Fig. 4(c) that low angle grain boundaries (LAGBs, <2°) are significantly reduced in comparison with those of as-received alloy. The volume fraction of recrystallized grains increases to 50% after DB process compared to that (32%) of as-received alloy.

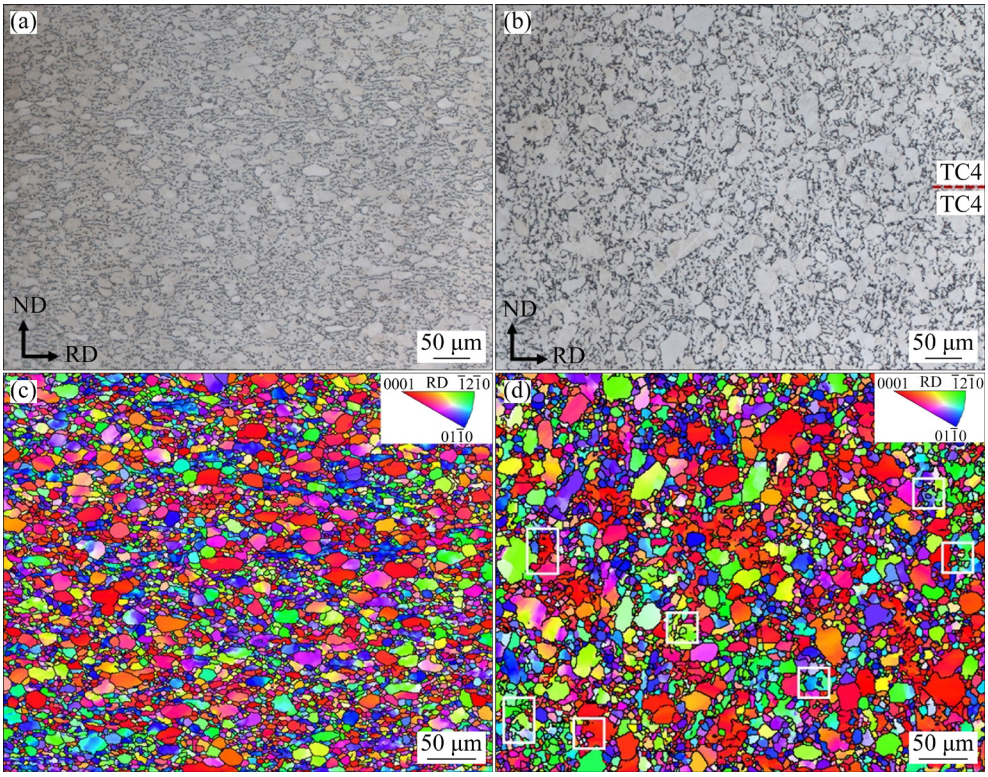

Fig. 3 OM (a, b) and EBSD orientation (c, d) images of as-received alloy and DB joint: (a, c) As-received alloy; (b, d) DB joint

Table 2 Statistics of grain size for as-received and DB TC4 titanium alloys (μm)

Phase	Thermal state	Average size	Standard deviation	Min. size	Max. size
α	As-received	5.2	3.7	0.8	23.2
	DB	6.7	6.3	1.1	66.4
β	As-received	1.1	0.3	0.8	2.6
	DB	1.8	0.6	1.1	4.8

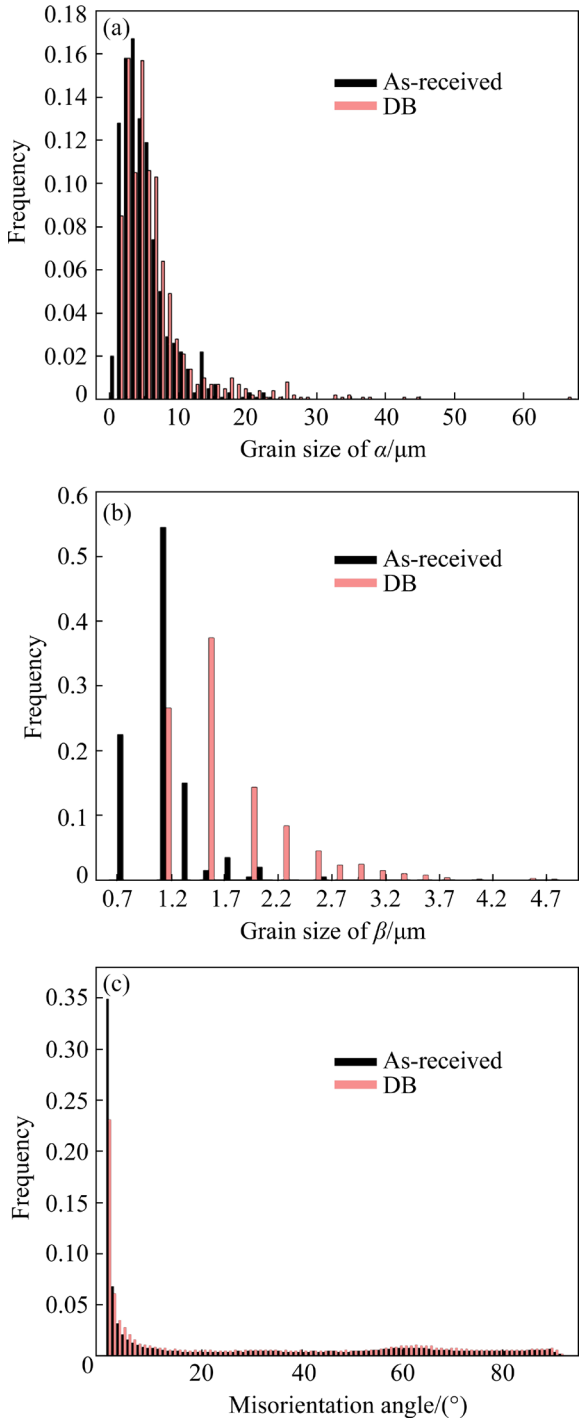

Fig. 4 Grain size distribution of α (a) and β (b) phases, and misorientation angle distribution (c) of as-received and DB alloys

Tensile and shear properties of as-received and diffusion-bonded TC4 titanium alloy are listed in Table 3. The yield strength, ultimate tensile strength, total elongation, and shear strength of diffusion bonded specimens slightly decrease compared with those of as-received specimens. It indicates the thermal cycling of DB process has a minor effect on static mechanical properties of TC4 titanium alloy.

Table 3 Tensile and shear properties of as-received alloy and DB joint

Thermal state	Yield strength/ MPa	Ultimate tensile strength/MPa	Total elongation/ %	Shear strength/ MPa
As-received	961±3	991±3	18.1±0.6	633±3
DB	946±4	961±5	11.3±0.8	625±3

3.2 Vibration fatigue life

The samples for vibration fatigue experiment were divided into two groups, Group A and Group B. Group A was subjected to a higher stress level, with the stress of DB and as-received specimens holding at 450 and 500 MPa, respectively. While for Group B, the stress of the two specimens gradually increased from 350 to 475 MPa, which was lower compared to that of Group A. The first-order natural frequencies of all the specimens are around 733 Hz. The fatigue lifetime results are presented in Table 4. DB specimen in Group B ($4^{\#}$) failed earlier than as-received one ($3^{\#}$) when subjected to the same stress level. Nevertheless, the number of cycles for DB specimen in Group A ($2^{\#}$) was still lower than that of as-received one ($1^{\#}$) even though it was subjected to a lower stress level.

Table 4 Vibration fatigue life data of two groups

Group No.	Thermal state	Stress/ MPa	Load cycles at single stress level	Total load cycles
A	As-received ($1^{\#}$)	500		155715
	DB ($2^{\#}$)	450		108788
B	As-received ($3^{\#}$)	350	3×10^7	5.03×10^7
		400	1×10^7	
		450	1×10^7	
		475	313440	
	DB ($4^{\#}$)	350	1×10^7	3.37×10^7
		400	1×10^7	
		450	1×10^7	
		475	3721695	

Hence, the vibration fatigue life deteriorates obviously after DB process.

The fatigue cracks of four specimens initiate on the surface near the circular segment as pointed by the red arrow in Fig. 5(a). The fatigue crack is quite macroscopically flat and its propagation direction is almost perpendicular to the maximum principal stress since the maximum principal stress on sample surface during vibration is parallel to RD. It accords to the general rules of high cycle fatigue crack propagation. Slight changes in crack propagation direction (marked by yellow arrows) can be seen using optical microscope as shown in Fig. 5(b). Further studies on crack paths and micro-voids near the main crack were carried out below.

3.2.1 Fatigue fracture surface

The fatigue fracture surfaces of as-received and DB specimens in Group B are shown in Fig. 6. The fracture region is clearly divided into two zones. As marked in Figs. 6(a, b), obvious fatigue lines and river patterns could be found in the fatigue fracture area (Region A). While Region B is the tensile fracture area induced by quasi-static tension in order to obtain final fracture. Cracks initiate on the surface of as-received and DB specimens as marked by black square in Figs. 6(a, b). Crack propagation direction (marked by white dashed arrows in Figs. 6(a, b) can be determined according to the morphology of the river patterns. The river patterns on both sides of the fatigue lines are obviously different in Fig. 6(c), and fracture surfaces gradually become rougher as the fatigue crack propagates. As shown in Fig. 6(d), the DB interface cannot be seen from the fracture section,

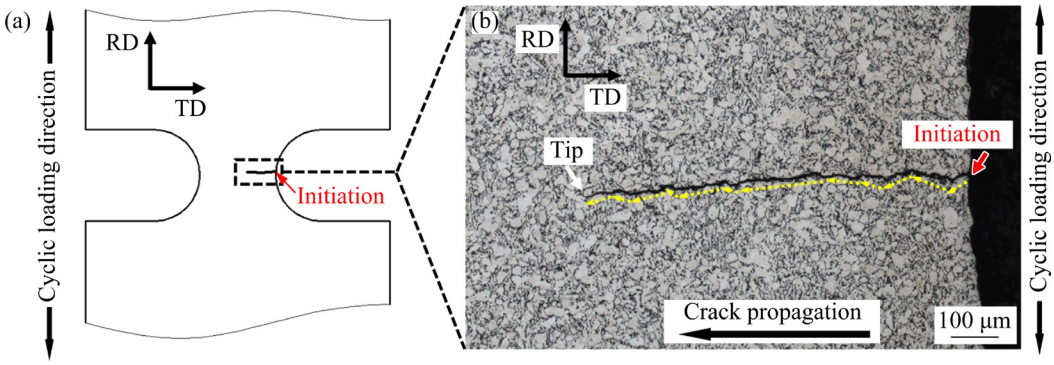

Fig. 5 Fatigue crack path: Schematic diagram (a); OM image of 2# DB specimen crack path in Group A (b) (The mark of "cyclic loading direction" refers to bending normal stress direction since the vibration movement of specimen tip is perpendicular to RD−TD plane)

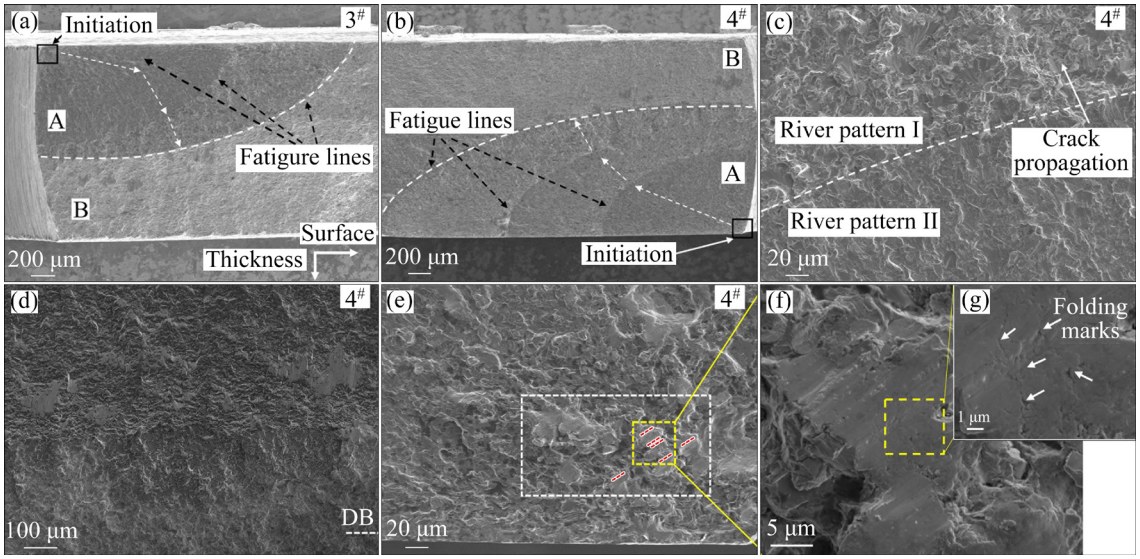

Fig. 6 Fatigue fracture surfaces: (a) 3# as-received specimen; (b) 4# DB specimen in Group B; (c) Different river patterns on both sides of fatigue line of 4# DB specimen; (d) Magnified facture characteristic near 4# DB interface; (e) Continuously distributed α-facets near crack initiation site of 4# DB specimen; (f, g) Facets at high magnifications

and the river patterns do not change their direction visibly when crossing DB interface. There are relatively coarse and continuously distributed α-facets close to the crack initiation site of DB specimen as marked by white dashed square in Fig. 6(e). Slip traces (highlighted by red dashed lines) with almost the same direction can be observed on these facets, where α grains with uniform orientation and larger average size may exist. Since the propagation resistance is much lower [33], crack propagation rate can increase if the grain orientation is nearly uniform and easy for slip activation. However, no similarly interconnected facets were found throughout the fatigue fracture surfaces of as-received specimen. Magnified observation of these fracture surfaces shows that there are some folding marks as shown in Figs. 6(f, g), which are formed by repetitive opening and closing of the two crack surfaces under high-frequency vibration load.

3.2.2 Fatigue crack propagation path

Fatigue cracks mainly propagate across the grains, such as the transgranular crack crossing Grains G1 and G2 in Fig. 7, which results from the minimal constraint on cyclic slip within the grain. Meanwhile, they sometimes propagate along α/α grain boundaries or α/β phase boundaries, such as the intergranular crack along with Grains G3, G4, and G5 in Fig. 7(a). Changes in crack propagation direction at micro level are relevant to α/β phase distributions. The formation of secondary cracks during the crack propagation is closely related to the aggregated β phase and similarly oriented α grains distributed along the crack path as circled in Fig. 7(b). All the secondary cracks are relatively short and ended at β phase, which indicates that hard β phase plays a hindering role in crack propagation.

The secondary cracks beneath the fracture surfaces were also observed. As shown in Fig. 8(a), secondary cracks mainly propagate inside α grains. When the secondary cracks encounter β grains, there is a significant hindrance for them to continuously propagate and expand into adjacent grains. A secondary crack at β grain tip and along α grain boundary (pointed by red arrow) can be clearly seen, and the schematic diagram is shown in Fig. 8(b).

4 Discussion

The effects of thermal cycling during DB process on the microstructure of TC4 titanium alloy were analyzed. In addition, the reasons for fatigue lifetime deterioration of diffusion bonded specimens were discussed according to the mechanisms of vibration fatigue crack initiation and propagation.

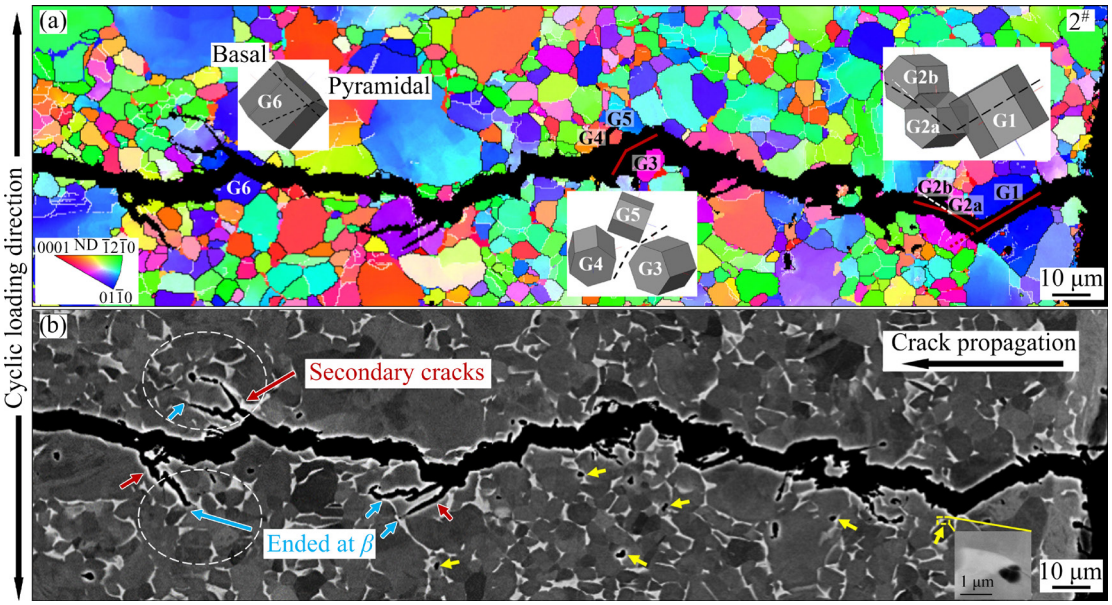

Fig. 7 Microstructures of fatigue crack path of 2# DB specimen in Group A: (a) EBSD orientation map with 3D orientation of Grains G1−G6; (b) BSE map (The white dashed circles mark aggregated β grains in the front of secondary cracks, and the blue arrows demonstrate secondary cracks that end at β grains. Micro-voids at α/β phase boundaries are highlighted by yellow arrows, and a magnified view of a micro-void is exhibited)

4.1 Grain size and orientation variations

DB process leads to the increase in average grain size and its inhomogeneity, as shown in Table 2. The reasons are explained as follows. Firstly, the specimen is gradually heated to 900 °C and held for 0.5 h, and then gradually cooled to room temperature in a vacuum furnace during DB thermal cycling process. The elevated temperature can promote grain growth. Secondly, the heating process contributes to static recrystallization. Thus, the LAGB percentage in DB specimens decreases since LAGBs merge to form the recrystallized nuclei, and the fraction of recrystallized grains increases. In a word, a combination of large grains due to the elevated temperature and relatively fine grains owing to the early stage of recrystallization exhibits the inhomogeneous grain size distribution. Grain growth can lead to an increase in effective slip length, which deteriorates fatigue lifetime according to Tanaka−Mura equation [34] for cyclic loading.

Grain orientation changes after thermal cycling process are shown in Fig. 9. The {0001} basal planes of as-received alloy are mostly perpendicular to RD, while they turn mostly perpendicularly to TD after DB process. Grain orientation evolution might result from the phase transformation of $\alpha \rightarrow \beta \rightarrow \alpha$ during thermal cycling process [35]. For titanium alloys, easy slip modes are $\vec{a}$ type $\langle 11\bar{2}0\rangle\{10\bar{1}0\}$ prismatic, $\langle 11\bar{2}0\rangle\{0001\}$ basal and $\langle 11\bar{2}0\rangle\{10\bar{1}1\}$ 1st order pyramidal. Most of the *c*-axis of grains in as-received alloy are nearly parallel to the loading direction, which results in both $\langle 11\bar{2}0\rangle\{0001\}$ basal and $\langle 11\bar{2}0\rangle\{10\bar{1}0\}$ prismatic slip systems being hard to activate. While $\langle 11\bar{2}0\rangle\{10\bar{1}0\}$ prismatic slip system is relatively dominant for DB specimens since {0001} basal planes are mostly parallel to the loading direction.

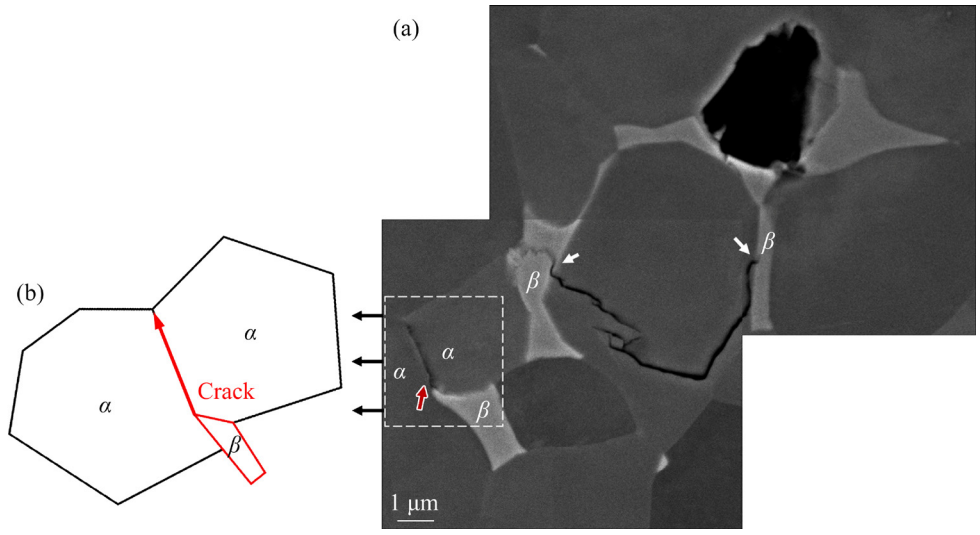

Fig. 8 Secondary cracks underneath fatigue fracture surface of 4# DB specimen in Group B: (a) BSE image; (b) Corresponding schematic diagram to illustrate crack at *β* grain tip and along *α* grain boundary

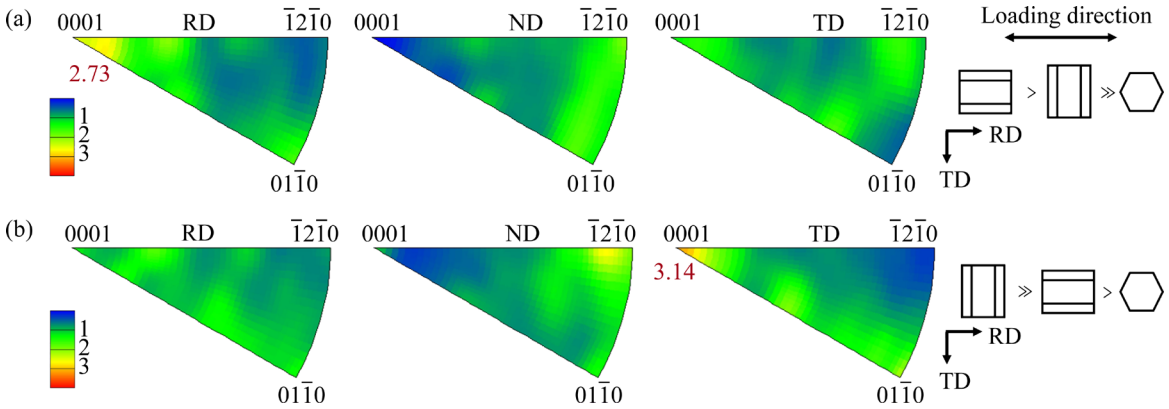

Fig. 9 Inverse pole figure maps and schematic diagram for related crystallographic orientation proportion of as-received (a) and DB (b) samples

The highest values of three possible Schmid factors for three slip systems, i.e., ⟨*a*⟩ basal, ⟨*a*⟩ prismatic and ⟨*a*⟩ pyramidal, obtained from EBSD analysis are presented in Fig. 10 for comparison. The percentage of grains that have higher prismatic slip Schmid factor significantly increases for DB specimen. The critical resolved shear stress (CRSS) corresponding to ⟨*a*⟩ prismatic, ⟨*a*⟩ basal and ⟨*a*⟩ pyramidal slip system is 370, 420 and 490 MPa for TC4 alloy, respectively [36]. When the Schmid factor is higher and corresponding CRSS is lower, the slip system is easier to be activated. Thus, dominant ⟨*a*⟩ prismatic slip system associated with lower CRSS in DB specimen might result in faster crack initiation and lower fatigue life compared to that in as-received alloy.

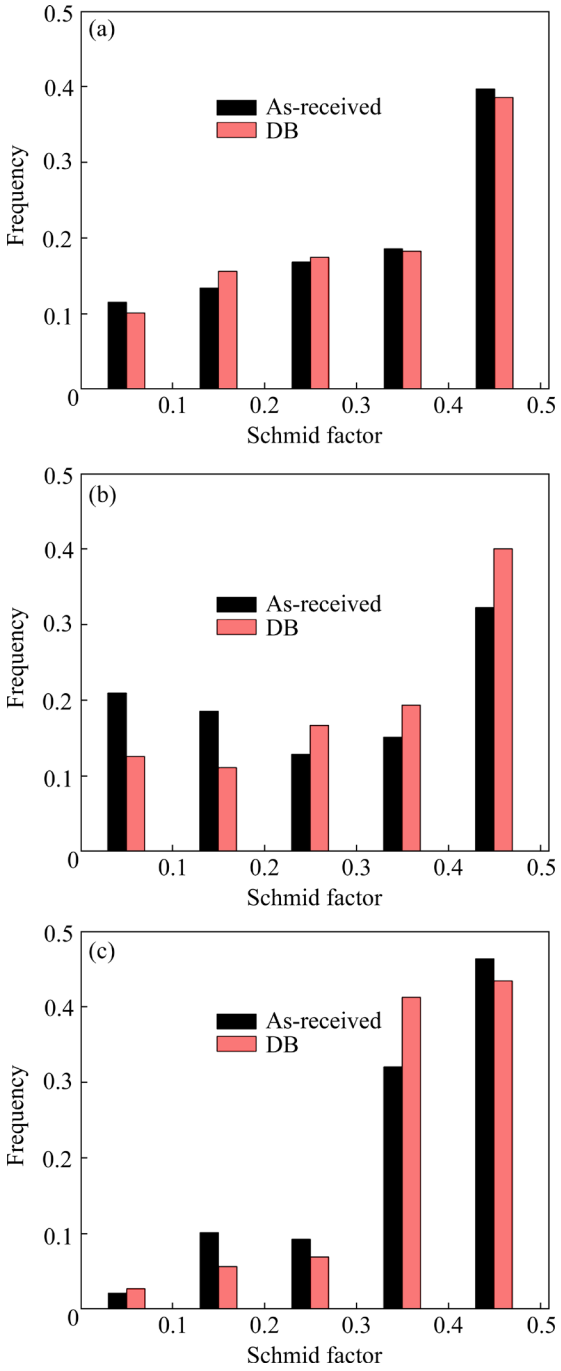

Fig. 10 Schmid factor (highest of all possible values) distribution of basal (a), prismatic (b), and pyramidal (c) slip modes for as-received and DB samples

In addition, the grain orientation also significantly affects fatigue crack propagation process and contributes to crack propagation direction changes at micro level. A favored "crack plane" is chosen during crack propagation according to grain orientation. As shown in Fig. 7(a), a deflection of about 60° occurs when the crack crosses from Grain G1 to Grain G2. The reason for obvious crack propagation path change is as follows. For Grain G1, the Schmid factor for basal slip (0.43) is higher than prismatic slip (0.11), thus the crack preferentially that for propagates along the basal plane. While for Grain G2, the Schmid factor for prismatic slip (0.44) is much higher than that for basal slip (0.06), causing the crack to propagate along the prismatic plane. Moreover, a small-angular deflection occurs when the crack crosses LAGBs inside Grain G2. It indicates that the crack propagation is highly sensitive to grain orientation. If multiple slip systems in a grain are easily activated, the crack may deflect within the grain, such as Grain G6 in Fig. 7(a) with both high Schmid factors for basal (0.49) and pyramidal (0.4) slip systems. The high sensitivity of crack to grain orientation can cause a frequent propagation direction change when it crosses fine grains due to the randomly distributed favored plane, which leads to a tortuous crack path and lower propagation rate. While for larger and soft-oriented grains with longer effective slip length and more easily activated slip systems in DB specimen, the crack might propagate faster.

4.2 Incompatible deformation for crack initiation

Micro-void is a direct manifestation of incompatible local deformation. Therefore, the fatigue crack initiation mechanism is indirectly discussed by analyzing the formation of micro-voids near the main crack during cyclic loading. As shown in Fig. 7(b), micro-voids exist mainly at three sites near the main fatigue crack: α/β phase boundaries, α/α grain boundaries and inside α grains. Micro-voids are most commonly located at

α/*β* phase boundaries as marked by yellow arrows in Fig. 7(b), followed by those inside *α* grains.

4.2.1 Voids at *α*/*β* phase boundaries

Since most of the micro-voids observed are located at *α*/*β* phase boundaries, it can be assumed that micro-voids tend to nucleate at phase boundaries. The lattice mismatch and strength difference between *α* and *β* phases cause a large number of dislocation pile-ups at *α*/*β* phase boundaries and make them the preferable sites for localizing plastic strain [37]. Furthermore, almost all of them tend to grow toward *α* phase, like Void-1 and Void-2 as shown in Fig. 11. The local stress concentration might activate more slip systems in *α* grain than those in *β* grain. As the number of loading cycles increases, micro-voids at the phase boundaries might gradually evolve into the cracks as observed in Fig. 8. The content of *β* phase increased by 38% after DB process, which provided more sites for micro-voids to nucleate and aggravated material damage.

4.2.2 Voids inside *α* grains

Micro-voids inside *α* grains often nucleate at the intersection of LAGBs during cyclic loading. The formation of LAGBs in *α* grains is mostly related to the deformation features of adjacent *α* grains and the distribution of surrounded *β* phase. As shown in Figs. 12(a−c), a void appears at the intersection of three LAGBs inside Grain G2. Schmid factors of prismatic and basal slip systems are 0.48 and 0.12 for Grain G1, respectively. In contrast, Schmid factors of prismatic and basal slip systems are 0.18 and 0.48 for Grain G2, separately. Due to the significant misorientation between these

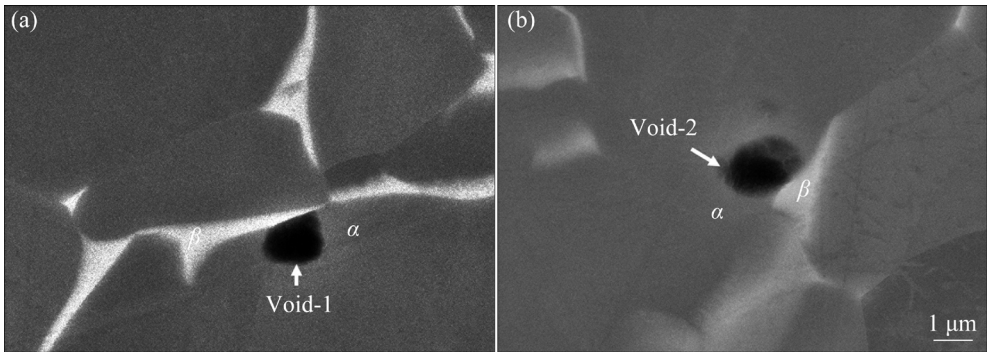

Fig. 11 Micro-voids of Void-1 (a) and Void-2 (b) at *α*/*β* phase boundaries of 2# DB specimen in Group A

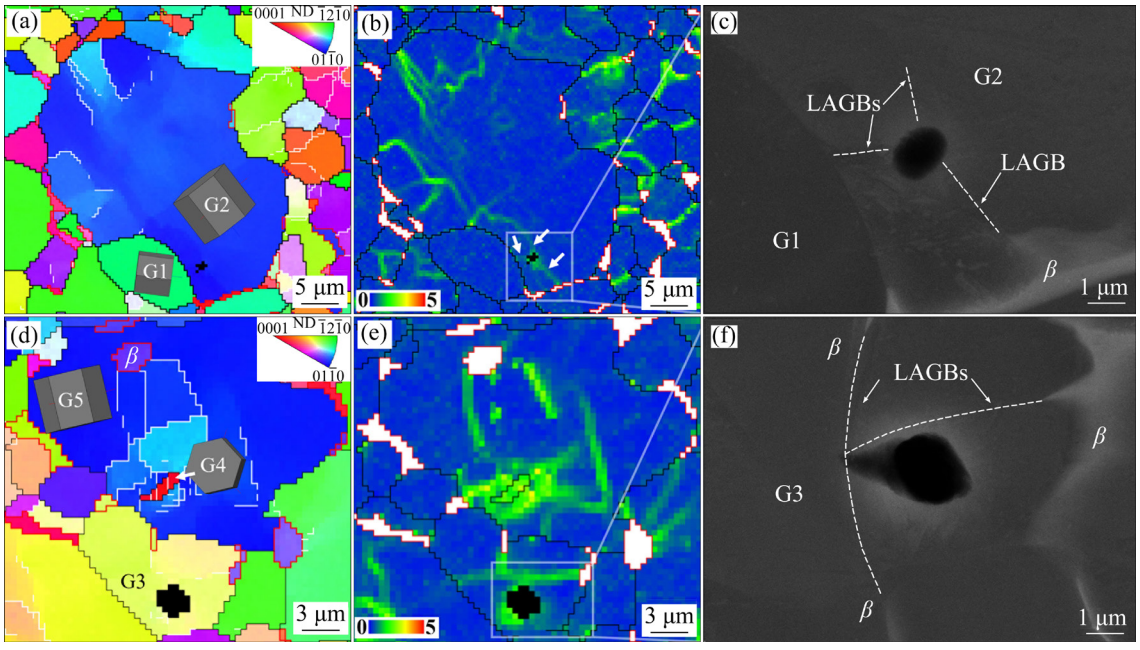

Fig. 12 Micro-voids inside *α* grains of 2# DB specimen in Group A: (a, d) EBSD orientation maps; (b, e) KAM maps for *α* grains; (c, f) Magnified BSE images of voids

two grains, the stacked dislocations at G1/G2 grain boundaries can activate the slip source in Grain G2 during cyclic loading [38,39]. In the meantime, the β phase distribution at the boundary of Grain G2 also contributes to the formation of LAGBs. Similarly, dislocation pile-ups at the tip of the surrounding β grains generate dislocation lines in Grain G3 in Fig. 12(f). The void nucleates at the junction of dislocation lines.

It should be noted that a small soft-oriented Grain G4, which might be caused by the recrystallization during DB thermal cycling process, is observed inside large Grain G5. The *c*-axis of Grain G4 is almost perpendicular to the loading direction, which means that prismatic slip system is dominant. However, Grain G5 is hard-oriented as its *c*-axis is nearly parallel to the loading direction. As observed in Fig. 12(e), kernel average misorientation (KAM) values of Grain G5 around G4 are much higher, and dislocation tangles are obvious. It indicates that the impeded dislocation migration through grain boundaries causes localized plastic deformation of Grain G5. Thus, deformation between recrystallized grains and large original grains might be out of consistency. Meanwhile, a β grain inside α grain is observed in Fig. 12(d), which is hardly found in as-received alloy. Due to $\alpha \rightarrow \beta$ phase transformation during heating process, β grains might nucleate both at grain boundaries and within α grains [40,41]. The β grain inside α grain clearly impeded the dislocation movement since a large number of LAGBs around β grain are observed, which might also contribute to micro-void nucleation inside α grains.

4.2.3 Voids at α/α grain boundary

Micro-voids at the α/α grain boundary in Fig. 13(a) are often caused by inconsistent deformation between hard and soft oriented grain pairs during cyclic loading. For example, Grain G1 in Fig. 13(a) is hard-oriented as it has low Schmid factors for both prismatic and basal slip systems, which means that it is hard to active slip system in Grain G1. In contrast, the Schmid factor (0.46) of basal slip is quite high for larger Grain G2. Direct dislocation transmission through boundaries of hard and soft-oriented grain pairs is quite difficult [40]. Thus, dislocation pile-ups at the grain boundary result in dislocation source activation in hard-oriented grain or void nucleation.

The grain size inhomogeneity increase after DB process often leads to a large α grain surrounded by many small and fine grains, such as

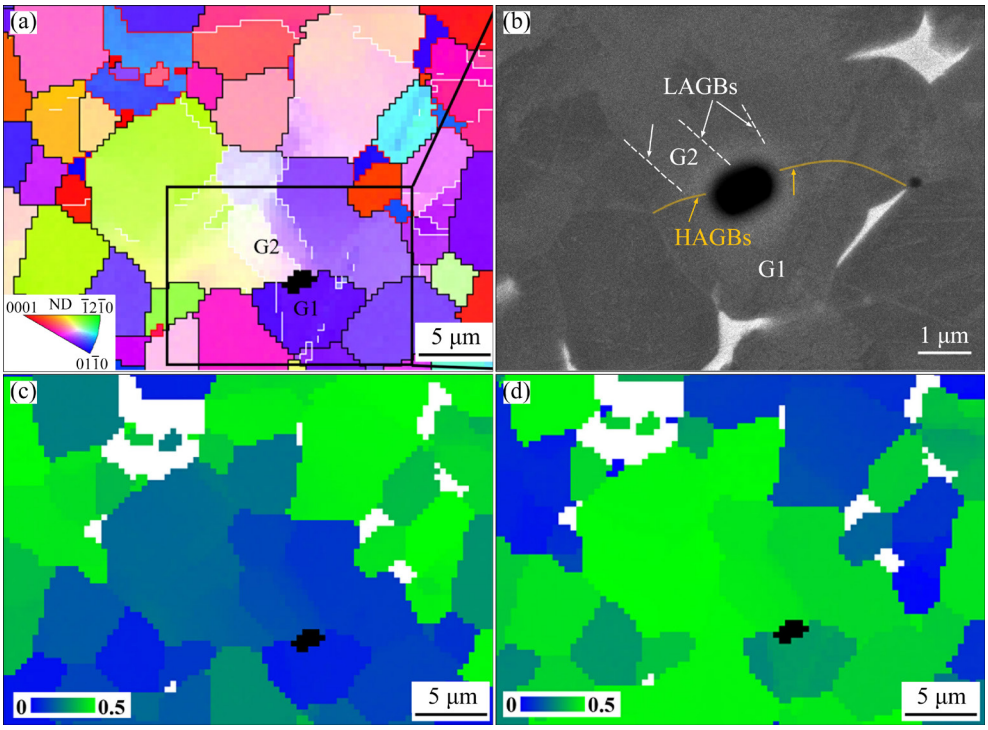

Fig. 13 Micro-void along α/α grain boundary of 2# DB specimen in Group A: (a) EBSD orientation map; (b) BSE image of magnified void view (HAGBs denote high angle grain boundaries); (c, d) Schmid factor distribution of prismatic and basal slips in α grains, respectively (white zones represent β grains)

Grain G2 in Fig. 12(a) and Fig. 13(a), which could be also found in Fig. 3(d). As schematically depicted in Fig. 14, the irreversible slip occurs on parallel slip planes of easily activated small grains or partially activated large grain. High local misorientation among partially activated large grain and hard-oriented small grains, or partially inactivated large grain and soft-oriented small grains can impede the direct dislocation transmission. Furthermore, it enhances plastic slip in soft-oriented grains and likely leads to void nucleation at α/α grain boundary, as the red voids shown in Fig. 14. Meanwhile, the surrounding small grains with different orientations drive the activation of multiple slip systems within the large grain to maintain deformation consistency around grain boundaries. However, this results in the formation of interlaced LAGBs inside large α grain, which further contributes to the nucleation of inside α void, as the green one shown in Fig. 14.

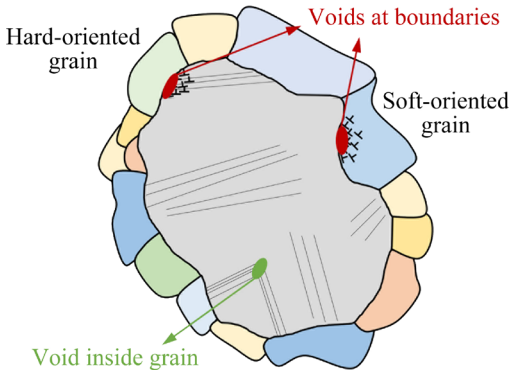

Fig. 14 Schematic illustration of boundary void (red) and inside-α void (green) formation

5 Conclusions

(1) Thermal cycling during DB process brings about significant microscopic change. Compared to as-received alloy, grain sizes in bonded TC4 titanium alloy become inhomogeneous as the grains grow. In addition, the volume fraction of β phase increases from 11.7% to 16.2% after DB process.

(2) After DB process, vibration fatigue lifetime of TC4 alloy deteriorates. The increase in grain size inhomogeneity due to thermal cycling promotes local cross-linkage of dislocation lines. Micro-voids nucleate at boundaries of small/large α grain pairs or inside large α grains. Meanwhile, grain orientation becomes conducive to prismatic slip after DB, which might also contribute to the earlier crack initiation.

(3) Aggregated β phase and similarly oriented α grain clusters near the main crack can facilitate the initiation of secondary cracks. The increased fraction of β phase stimulates LAGBs formation inside α grains and provides more locations for micro-voids nucleation.

CRediT authorship contribution statement

Yi-wen LEI: Conceptualization, Methodology, Investigation, Formal analysis, Data curation, Writing – Original draft preparation; **Guang-lu MA:** Visualization; **Yue LIU:** Validation; **Wei ZHAO:** Data curation; **Hui-ping WU:** Writing − Reviewing & editing; **Xi-feng LI:** Investigation, Resources, Writing − Reviewing & editing, Supervision, Funding acquisition.

Declaration of competing interest

The authors declare that they have no known competing financial interests or personal relationships that could have appeared to influence the work reported in this paper.

Acknowledgments

The authors gratefully appreciate financial support from the National Natural Science Foundation of China (Nos. 51875350, 52105383).

References

[1] BANERJEE D, WILLIAMS J C. Perspectives on titanium science and technology [J]. Acta Materialia, 2013, 61: 844−879.

[2] GERD L, JAMES C W. Titanium [M]. Berlin: Springer, 2007.

[3] XU Jian-wei, ZHENG Wei-dong, ZHOU Da-di, HE Sheng-tong, JIA Run-chen. Evolution of coordination between α and β phases for two-phase titanium alloy during hot working [J]. Transactions of Nonferrous Metals Society of China, 2021, 31: 3428−3438.

[4] LAINÉ S J, KNOWLES K M, DOORBAR P J, CUTTS R D, RUGG D. Microstructural characterisation of metallic shot peened and laser shock peened Ti−6Al−4V [J]. Acta Materialia, 2017, 123: 350−361.

[5] PAN Xin-lei, HE Wei-feng, HUANG Xuan, WANG Xue-de, SHI Xiao-song, JIA Wen-tong, ZHOU Liu-cheng. Plastic deformation behavior of titanium alloy by warm laser shock peening: Microstructure evolution and mechanical properties [J]. Surface and Coatings Technology, 2021, 405: 126670.

[6] ZHAO Si-han, YUAN Kang-bo, GUO Wei-guo, HE Yan, XU Yu-heng, LIN Xin. A comparative study of laser metal deposited and forged Ti−6Al−4V alloy: Uniaxial mechanical response and vibration fatigue properties [J]. International Journal of Fatigue, 2020, 136: 105629.

[7] WITEK L. Crack propagation analysis of mechanically damaged compressor blades subjected to high cycle fatigue [J]. Engineering Failure Analysis, 2011, 18: 1223−1232.

[8] FENG Guang-jie, WEI Yan, HU Bing-xu, WANG Yi-feng, DENG De-an, YANG Xiu-xia. Vacuum diffusion bonding of Ti2AlNb alloy and TC4 alloy [J]. Transactions of Nonferrous Metals Society of China, 2021, 31: 2677−2686.

[9] DENG Wu-jing, SHAO Jie, CHEN Wei, LI Zhi-qiang, LI Xiao-hua. Influence of interface defect on high cycle fatigue behavior of titanium alloy diffusion bonding joint [J]. Aeronautical Manufacturing Technology, 2020, 63(22): 78−83. (in Chinese)

[10] HE Xiao-fan, DONG Ying-hao, LI Yu-hai, WANG Xiang-ming. Fatigue crack growth in diffusion-bonded Ti−6Al−4V laminate with unbonded zones [J]. International Journal of Fatigue, 2018, 106: 1−10.

[11] LI Shu-xin, XUAN Fu-zhen, TU Shan-tung. Fatigue damage of stainless steel diffusion-bonded joints [J]. Materials Science and Engineering A, 2008, 480: 125−129.

[12] LI Tian-le, WU Hui-ping, WANG Bin, LI Sheng, LI Xi-feng, CHEN Jun. Fatigue crack growth behavior of TA15/TC4 dissimilar laminates fabricated by diffusion bonding [J]. International Journal of Fatigue, 2022, 156: 106646.

[13] LI Hong, LI Miao-quan, YU Wei-xin, LIU Hong-bin. Significance and interaction of bonding parameters with bonding ratio in press bonding of TC4 alloy [J]. Rare Metals, 2016, 35: 235−241.

[14] WU Hui-ping, LI Xi-feng, MEI Qiong-feng, CHEN Jun, WU Guo-hong. Flow behavior of diffusion bonding interface of Ti_6Al_4V alloy over a wide range of strain rates [J]. Materials Science and Engineering A, 2019, 761: 138067.

[15] ZHANG Hao, LI Jing-hong, MA Ping-yi, XIONG Jiang-tao, ZHANG Fu-sheng. Study on microstructure and impact toughness of TC4 titanium alloy diffusion bonding joint [J]. Vacuum, 2018, 152: 272−277.

[16] CALVO F A, de SALAZAR J M G, UREÑA A, CARRIÓN J G, PEROSANZ F. Diffusion bonding of Ti−6Al−4V alloy at low temperature: Metallurgical aspects [J]. Journal of Materials Science, 1992, 27: 391−398.

[17] CAPPOLA J, STINVILLE J C, CHARPAGNE M A, CALLAHAN P G, ECHLIN M P, POLLOCK T M, PILCHAK A, KASEMER M. On the localization of plastic strain in microtextured regions of Ti−6Al−4V [J]. Acta Materialia, 2021, 204: 116492.

[18] CHEN Kui-wai, PAN Su-ping, LIU Hui-qun, JIANG Yong. Effect of α phase morphology on fatigue crack growth behavior of Ti−5Al−5Mo−5V−1Cr−1Fe alloy [J]. Transactions of Nonferrous Metals Society of China, 2020, 30: 2459−2471.

[19] LUCAS J J, KONIECZNY P P. Relationship between alpha grain size and crack initiation fatigue strength in Ti−6Al−4V [J]. Metallurgical Transactions, 1971, 2: 911−912.

[20] ZUO Jing-hui, WANG Zhong-guang, HAN En-hou. Effect of microstructure on ultra-high cycle fatigue behavior of Ti−6Al−4V [J]. Materials Science and Engineering A, 2008, 473: 147−152.

[21] NARAGANI D, SANGID M D, SHADE P A, SCHUREN J C, SHARMA H, PARK J S, KENESEI P, BERNIER J V, TURNER T J, PARR I. Investigation of fatigue crack initiation from a non-metallic inclusion via high energy X-ray diffraction microscopy [J]. Acta Materialia, 2017, 137: 71−84.

[22] SANGID M D, MAIER H J, SEHITOGLU H. An energy-based microstructure model to account for fatigue scatter in polycrystals [J]. Journal of the Mechanics and Physics of Solids, 2011, 59: 595−609.

[23] ANKEM S, MARGOLIN H. A rationalization of stress-strain behavior of two-ductile phase alloys [J]. Metallurgical Transactions A, 1986, 17: 2209−2226.

[24] HÉMERY S, STINVILLE J C. Microstructural and load hold effects on small fatigue crack growth in $\alpha+\beta$ dual phase Ti alloys [J]. International Journal of Fatigue, 2022, 156: 106699.

[25] TAN Chang-sheng, SUN Qian-yan, XIAO Lin, ZHAO Yong-qing, SUN Jun. Slip transmission behavior across α/β interface and strength prediction with a modified rule of mixtures in TC21 titanium alloy [J]. Journal of Alloys and Compounds, 2017, 724: 112−120.

[26] SHI Yi, YANG Xiao-guang, MIAO Guo-lei, SHI Duo-qi. Experimental investigation of micro crack initiation based on digital image correlation method [J]. Journal of Propulsion Technology, 2022, 40(7): 1606−1612. (in Chinese)

[27] LI Shan-lin, LIU Qu, RUI Shao-shi, LI Xiao-gang, HU Meng-jia, LI Ke-jian, SUN Qi-xing, CAI Zhi-peng, PAN Ji-luan. Fatigue crack initiation behaviors around defects induced by welding thermal cycle in superalloy IN617B [J]. International Journal of Fatigue, 2022, 158: 106745.

[28] JIANG R, BULL D J, EVANGELOU A, HARTE A, PIERRON F, SINCLAIR I, PREUSS M, HU X T, REED P A S. Strain accumulation and fatigue crack initiation at pores and carbides in a SX superalloy at room temperature [J]. International Journal of Fatigue, 2018, 114: 22−33.

[29] WANG Zhang-dong, WANG Shi-bin, YANG Kun, CHEN Ming-zhi, BI Ke-dong, NI Zhong-hua, SUN Gui-fang. In-situ SEM investigation on the fatigue behavior of Ti−6Al−4V ELI fabricated by the powder-blown underwater directed energy deposition technique [J]. Materials Science and Engineering A, 2022, 838: 142783.

[30] ZHOU Jian-li, REN Xiao-yi, ZHANG Yi-xu, WANG Jin, ZHANG Yue-fei, ZHANG Ze. Research on in situ high temperature fatigue test method based on scanning electron microscope [J]. Journal of Chinese Electron Microscopy Society, 2021, 40(3): 215−220. (in Chinese)

[31] GAO Tao, XUE Hong-qian, SUN Zhi-dan, RETRAINT D, HE Yan-li. Micromechanisms of crack initiation of a Ti−8Al−1Mo−1V alloy in the very high cycle fatigue regime [J]. International Journal of Fatigue, 2021, 150: 106314.

[32] de SALVO J G J, AFONSO C R M. Fatigue strength and microstructure evaluation of Al 7050 alloy wires recycled by spray forming, extrusion and rotary swaging [J]. Transactions of Nonferrous Metals Society of China, 2020, 30: 3195−3209.

[33] NALLA R K, RITCHIE R O, BOYCE B L, CAMPBELL J P, PETERS J O. Influence of microstructure on high-cycle fatigue of Ti−6Al−4V: Bimodal vs. lamellar structures [J]. Metallurgical and Materials Transactions A, 2002, 33: 899−918.

[34] TANAKA K, MURA T. A dislocation model for fatigue

crack initiation [J]. Journal of Applied Mechanics, 1981, 48: 97−103.
[35] CEPEDA-JIMÉNEZ C M, OROZCO-CABALLERO A, SARKEEVA A, KRUGLOV A, LUTFULLIN R, RUANO O A, CARREÑO F. Effect of processing temperature on the texture and shear mechanical properties of diffusion bonded Ti−6Al−4V multilayer laminates [J]. Metallurgical and Materials Transactions A, 2013, 44: 4743−4753.
[36] BRIDIER F, MCDOWELL D L, VILLECHAISE P, MENDEZ J. Crystal plasticity modeling of slip activity in Ti−6Al−4V under high cycle fatigue loading [J]. International Journal of Plasticity, 2009, 25: 1066−1082.
[37] TAN Chang-sheng, SUN Qiao-yuan, XIAO Lin, ZHAO Yong-qing, SUN Jun. Cyclic deformation and microcrack initiation during stress controlled high cycle fatigue of a titanium alloy [J]. Materials Science and Engineering A, 2018, 711: 212−222.
[38] JOSEPH S, LINDLEY T C, DYE D. Dislocation interactions and crack nucleation in a fatigued near-alpha titanium alloy [J]. International Journal of Plasticity, 2018, 110: 38−56.
[39] ZHENG Z B, BALINT D S, DUNNE F P E. Investigation of slip transfer across HCP grain boundaries with application to cold dwell facet fatigue [J]. Acta Materialia, 2017, 127: 43−53.
[40] JOSEPH S, BANTOUNAS I, LINDLEY T C, DYE D. Slip transfer and deformation structures resulting from the low cycle fatigue of near-alpha titanium alloy Ti−6242Si [J]. International Journal of Plasticity, 2018, 100: 90−103.
[41] SEWARD G G E, CELOTTO S, PRIOR D J, WHEELER J, POND R C. In situ SEM-EBSD observations of the hcp to bcc phase transformation in commercially pure titanium [J]. Acta Materialia, 2004, 52: 821−832.

TC4 钛合金扩散连接接头的振动疲劳特性及劣化机理

雷奕文[1]，马广璐[2]，刘 悦[2]，赵 伟[2]，吴会平[1]，李细锋[1]

1. 上海交通大学 材料科学与工程学院 塑性成形技术与装备研究院，上海 200030；
2. 沈阳黎明航空发动机有限责任公司，沈阳 110043

摘 要：为了研究扩散连接工艺对材料振动疲劳特性的影响，对扩散连接后的 TC4 钛合金和原始母材进行一系列振动疲劳试验以及显微组织表征。结果表明：扩散连接的热循环过程引起 TC4 钛合金显微组织变化，并导致其振动疲劳性能降低。经扩散连接后，TC4 钛合金晶粒尺寸的不均匀性增加，加重了材料不同取向 α 晶粒间的不协调变形，从而使微孔洞易于在晶粒尺寸差异较大的两 α 晶粒的晶界上萌生，或者在较大 α 晶粒的内部萌生。同时，扩散连接后材料 α 晶粒取向的变化使得柱面滑移系更易被启动，促进了裂纹更早地萌生。此外，扩散连接后 TC4 钛合金 β 相含量的增加为微孔洞提供了更多的形核位置。因此，由扩散连接热循环过程造成的晶粒尺寸不均匀性增加、晶粒取向变化和 β 相含量增加使扩散连接 TC4 钛合金的振动疲劳性能劣化。

关键词：扩散连接；振动疲劳；热循环；TC4 钛合金

(Edited by Wei-ping CHEN)